

System 1&2 Synergy via Dynamic Model Interpolation

Chenxu Yang^{1,2*}, Qingyi Si^{3*}, Chong Tian⁴, Xiyu Liu^{1,2}, Dingyu Yao^{1,2},
 Chuanyu Qin^{1,2}, Zheng Lin^{1,2†}, Weiping Wang¹, Jiaqi Wang³,

¹Institute of Information Engineering, Chinese Academy of Sciences, Beijing, China

²School of Cyber Security, University of Chinese Academy of Sciences, Beijing, China

³JD.COM ⁴MBZUAI

{yangchenxu,linzheng}@iie.ac.cn

Abstract

Training a unified language model that adapts between intuitive System 1 and deliberative System 2 remains challenging due to interference between their cognitive modes. Recent studies have thus pursued making System 2 models more efficient. However, these approaches focused on output control, limiting what models produce. We argue that this paradigm is misaligned: output length is merely a symptom of the model’s cognitive configuration, not the root cause. In this work, we shift the focus to capability control, which modulates *how models think* rather than *what they produce*. To realize this, we leverage existing Instruct and Thinking checkpoints through dynamic parameter interpolation, without additional training. Our pilot study establishes that linear interpolation yields a convex, monotonic Pareto frontier, underpinned by representation continuity and structural connectivity. Building on this, we propose **DAMI** (DynAmic Model Interpolation), a framework that estimates a query-specific Reasoning Intensity $\lambda(q)$ to configure cognitive depth. For training-based estimation, we develop a preference learning method encoding accuracy and efficiency criteria. For zero-shot deployment, we introduce a confidence-based method leveraging inter-model cognitive discrepancy. Experiments on five mathematical reasoning benchmarks demonstrate that DAMI achieves higher accuracy than the Thinking model while remaining efficient, effectively combining the efficiency of System 1 with the reasoning depth of System 2.

1 Introduction

The cognitive evolution of Large Language Models (LLMs) has established a functional dichotomy: lightweight “System 1” models excel at rapid, intuitive responses, while “System 2” models such as OpenAI’s o1 [OpenAI, 2024] and DeepSeek-R1 [DeepSeek-AI *et al.*, 2025] achieve superior reasoning through extended Chain-of-Thought (CoT)

* Equal Contribution

† Zheng Lin is the corresponding author.

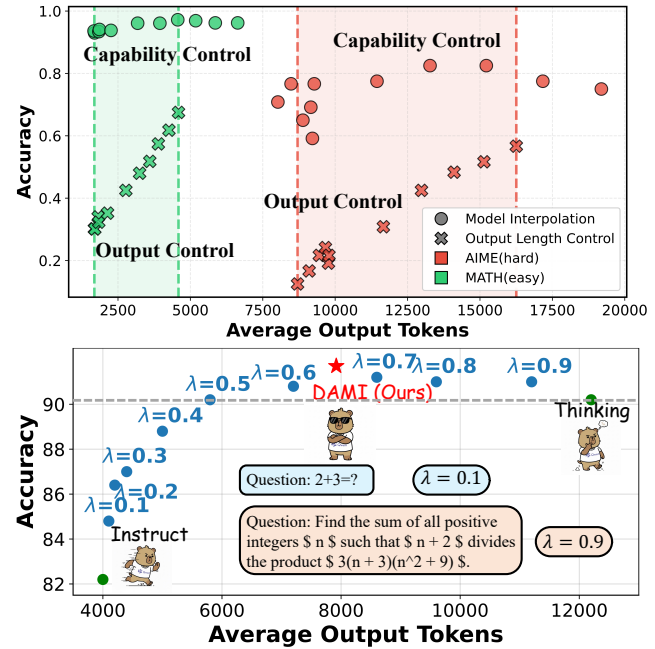


Figure 1: Capability control outperforms output control across different efficiency levels on both tasks. Linear interpolation between Instruct and Thinking yields a monotonic Pareto frontier.

[Li *et al.*, 2025]. Ideally, a unified model would seamlessly adapt between these modes, responding swiftly to simple queries while engaging deep deliberation for complex problems [Team, 2025]. However, training such an adaptive model remains an open challenge due to the zero-sum nature of training data [Shukor *et al.*, 2025]. The verbose, self-reflective style of System 2 reasoning conflicts with the concise responses of System 1, causing mutual interference during joint optimization. Consequently, state-of-the-art LLMs typically release separate Thinking and Instruct checkpoints rather than a single unified model [Bai *et al.*, 2025].

Given this difficulty, the community has pursued a more tractable alternative: making System 2 models more efficient. This pursuit has spawned various approaches, from training-free methods like token budgeting [Han *et al.*, 2025], early exit [Yang *et al.*, 2025c], and CoT compression [Xia *et al.*,

2025], to training-based methods employing reinforcement learning (RL) with length penalties [Arora and Zanette, 2025; Su and Cardie, 2025] or trajectory pruning [Dai *et al.*, 2025; Hou *et al.*, 2025]. Despite their diversity, these approaches share a common paradigm: **output control**, which limits *what* models produce. We argue that this framing is misaligned: output length is merely a symptom of the model’s cognitive configuration, not the root cause of inefficiency. As illustrated in Figure 1, constraining generation with token budgets risks truncating the reasoning process, resulting in incomplete chains of thought that severely degrade performance on challenging tasks.

In this work, we shift the focus from output control to **capability control**, which modulates *how models think* rather than *what they produce*. Our key observation is that by interpolating parameters between existing System 1 and System 2 checkpoints, we can smoothly adjust the model’s cognitive intensity without additional training. As shown in Figure 1 (upper), under comparable efficiency constraints, capability control consistently outperforms output control by producing naturally concise yet complete solutions.

A natural question arises: does parameter interpolation yield predictable behavior? Our pilot experiments in Section 3.1 provide affirmative evidence. We find that increasing the interpolation coefficient λ (where $\lambda=0$ corresponds to Instruct and $\lambda=1$ to Thinking) produces a smooth, monotonic Pareto frontier between accuracy and efficiency, as shown in Figure 1 (lower), with continuous transitions in representation space. This predictability is grounded in the structural similarity between models: cosine similarity exceeds 0.99 across all layers, indicating that both models satisfy Linear Mode Connectivity [Frankle *et al.*, 2020] and reside within the same optimization basin. These findings establish parameter interpolation as a principled mechanism for capability control.

Building on this foundation, we propose **DAMI** (DynAmic Model Interpolation), a framework that dynamically estimates a query-specific Reasoning Intensity $\lambda(q) \in [0, 1]$ to configure the model’s cognitive depth for each input. We explore two complementary methods tailored for different deployment scenarios: DAMI-Pref, a preference learning method that jointly encodes accuracy and efficiency criteria, is suited for accuracy-critical applications where in-domain training data is available; DAMI-Conf, a confidence-based method that leverages inter-model cognitive discrepancy, enables rapid deployment across diverse domains without requiring any training data. Experiments on five mathematical reasoning benchmarks show that DAMI improves accuracy by 1.6–3.4% while reducing token consumption by 29–40% compared to the Thinking model, outperforming static merging, early-exit, and routing baselines.

Our contributions are summarized as follows:

- We advocate a paradigm shift from output control to capability control for efficient reasoning, and identify dynamic model interpolation as a low-cost realization that leverages existing checkpoints, bypassing the difficulty of training System 1&2 unified models
- We propose DAMI with two complementary $\lambda(q)$ estimation methods: preference-based learning for data-

available scenarios and confidence-based inference for zero-shot deployment.

- Extensive experiments demonstrate that DAMI consistently establishes superior Pareto frontiers across diverse benchmarks and model families.

2 Related Work

2.1 Efficient Reasoning

The inherent trade-off between System 1’s efficiency and System 2’s accuracy has motivated a growing body of research on efficient reasoning, which can be categorized into single-model optimization and multi-model collaboration. Single-model approaches include early-exit methods that terminate generation upon sufficient confidence [Yang *et al.*, 2025c; Dai *et al.*, 2025], CoT compression that removes redundant reasoning steps [Xia *et al.*, 2025], adaptive reasoning that adjusts output length based on query complexity [Luo *et al.*, 2025; Shen *et al.*, 2025], and other trajectory-revised methods [Yang *et al.*, 2025b]. While adaptive methods share our motivation, they rely on RL with length penalties, incurring high training costs and potential performance degradation on difficult problems. Despite their diversity, these single-model approaches predominantly follow the output control paradigm, constraining *what* models produce. Multi-model approaches leverage complementary capabilities across models. Task decomposition methods delegate simple steps to lightweight models while reserving complex reasoning for stronger ones [Akhauri *et al.*, 2025; Fan *et al.*, 2025]. LLM Routing dynamically dispatches queries to suitable models from a pool [Ong *et al.*, 2025; Zhang *et al.*, 2025]. Model merging statically integrates parameters of different models to combine their strengths [Wu *et al.*, 2025a; Yao *et al.*, 2025b]. **Our work bridges routing and merging by enabling continuous, query-adaptive interpolation** rather than discrete model selection or static merging.

2.2 Model Merging

Model merging integrates parameters from multiple specialized models into a unified model without requiring original training data. It has been applied to mitigate catastrophic forgetting in continual learning [Schumann *et al.*, 2023], integrate knowledge in multi-task learning [Yang *et al.*, 2024; Ilharco *et al.*, 2023], and aggregate updates in federated learning [Wang *et al.*, 2020]. Recent work has introduced merging into efficient reasoning, with leading LLM teams releasing merged models that balance reasoning depth and efficiency [Wu *et al.*, 2025b; Team *et al.*, 2025; Wang *et al.*, 2023; Yang *et al.*, 2025a]. However, existing approaches apply fixed merging coefficients across all queries. To our knowledge, we are the first to propose query-aware dynamic merging between System 1 and System 2 models, enabling fine-grained integration of their complementary strengths for adaptive control over reasoning depth.

3 Methodology

3.1 Why Interpolation Enable Capability Control

Before formulating our dynamic framework, we first validate that parameter interpolation can serve as a continuous and

predictable control mechanism for reasoning. We conduct a pilot study using static linear interpolation between the Instruct model $\Theta^{(I)}$ and the Thinking model $\Theta^{(T)}$ with a fixed coefficient $\lambda \in [0, 1]$ across the test set.

$$\Theta^{(M)} = \lambda\Theta^{(T)} + (1 - \lambda)\Theta^{(I)} \quad (1)$$

Performance Monotonicity. As shown in Figure 1, increasing λ from 0 to 0.9 yields a smooth improvement in accuracy alongside a predictable increase in token consumption. Crucially, this trajectory forms a convex Pareto frontier where intermediate interpolations can outperform both endpoints: achieving higher accuracy than the Instruct model while requiring fewer tokens than the Thinking model. This confirms that λ serves as a reliable proxy for reasoning depth, enabling fine-grained efficiency-accuracy trade-offs.

Representation Continuity. What underlies this behavioral smoothness? We analyze the hidden states of `<think>` token using Principal Component Analysis (PCA) across 50 samples on the MATH-500. As shown in Figure 2(a), representations of interpolated models form a continuous trajectory connecting the Instruct and Thinking endpoints. The first principal component strongly correlates with λ ($r=0.974$), indicating that interpolation induces a gradual cognitive transition rather than discrete jumps in the representation space.

Structural Connectivity. This representational continuity is grounded in the geometric properties of the parameter space. Figure 2(b) shows that the Instruct and Thinking models maintain high cosine similarity (>0.99) across all transformer layers, satisfying the Linear Mode Connectivity (LMC) property [Frankle *et al.*, 2020; Zhan *et al.*, 2025]. This indicates that both models reside within the same optimization basin, ensuring that interpolation traverses a valid path in the loss landscape. Notably, the L2 distance peaks in middle-to-deep layers, suggesting that System 2 capabilities are encoded through targeted modifications in these regions rather than global parameter shifts.

Key Insight. These findings establish a causal chain: structural alignment in parameter space \rightarrow continuous transitions in representation space \rightarrow monotonic Pareto frontier in performance. This connectivity transforms reasoning resource allocation into a well-posed prediction problem, where estimating the optimal $\lambda(q)$ directly determines model behavior. We provide formal theoretical justifications for each component of this causal chain, including proofs for interpolation validity (Appendix A.1), performance monotonicity (Appendix A.2), and representation continuity (Appendix A.3). Together, these properties ensure that model interpolation behaves predictably and monotonically, providing the theoretical foundation for fine-grained, query-level dynamic merging. This validates our core premise: λ can serve as a reliable control knob for reasoning intensity, enabling the adaptive framework we introduce next.

3.2 The Dynamic Interpolation Framework

While Section 3.1 validates that parameter interpolation provides a reliable control mechanism, a fixed λ is inherently suboptimal since different queries require different reasoning

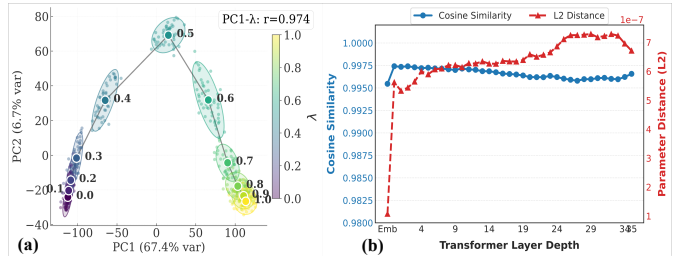


Figure 2: The monotonicity and continuity of reasoning intensity.

depths. DAMI addresses this by making λ query-dependent:

$$\Theta^{(M)}(q) = \lambda(q)\Theta^{(T)} + (1 - \lambda(q))\Theta^{(I)} \quad (2)$$

We term $\lambda(q) \in [0, 1]$ the **Reasoning Intensity**, which modulates the cognitive depth for each input. The key technical challenge is estimating the optimal $\lambda(q)$. We explore two complementary methods: **DAMI-Pref**, a preference learning approach that jointly encodes accuracy and efficiency criteria, suited for accuracy-critical applications where in-domain training data is available; and **DAMI-Conf**, a confidence-based approach that leverages inter-model cognitive discrepancy, enabling rapid deployment across diverse domains without requiring any training data.

3.3 Training-based Estimation of λ

Baseline: Regression-based Estimation

A straightforward solution is to train a lightweight router model R_ϕ to regress a pre-computed target $\lambda^*(q)$. We profile each query q across J discrete coefficients $\Lambda = \{l_1, \dots, l_J\}$, measuring accuracy via N -sample evaluation:

$$\text{Acc}^{l_j}(q) = \frac{1}{N} \sum_{n=1}^N \mathbb{I}(\mathcal{M}_n^{l_j}(q), a) \quad (3)$$

where $\mathcal{M}_n^{l_j}(q)$ is the response from a model merged with coefficient l_j , and $\mathbb{I}(\cdot, \cdot)$ is a binary evaluation function. The target $\lambda^*(q)$ is defined as the minimum coefficient achieving the highest accuracy, and the router is trained with MSE loss:

$$\mathcal{L}(\phi) = \frac{1}{|\mathcal{D}_{\text{train}}|} \sum_{q \in \mathcal{D}_{\text{train}}} (R_\phi(q) - \lambda^*(q))^2 \quad (4)$$

However, this approach suffers from two weaknesses: (1) point-wise labels $\lambda^*(q)$ are inherently noisy due to sampling variance, and (2) regression requires large-scale data for robust generalization. These limitations motivate our preference-based method.

DAMI-Pref: Preference-based Estimation

Instead of regressing noisy labels, we recast λ estimation as a preference learning problem. A lightweight reward model R_ψ is trained to score the relative efficacy of different coefficients, offering three advantages: (1) pairwise comparisons are more robust to noise, (2) preference criteria can jointly encode accuracy and efficiency, and (3) the method requires substantially less training data.

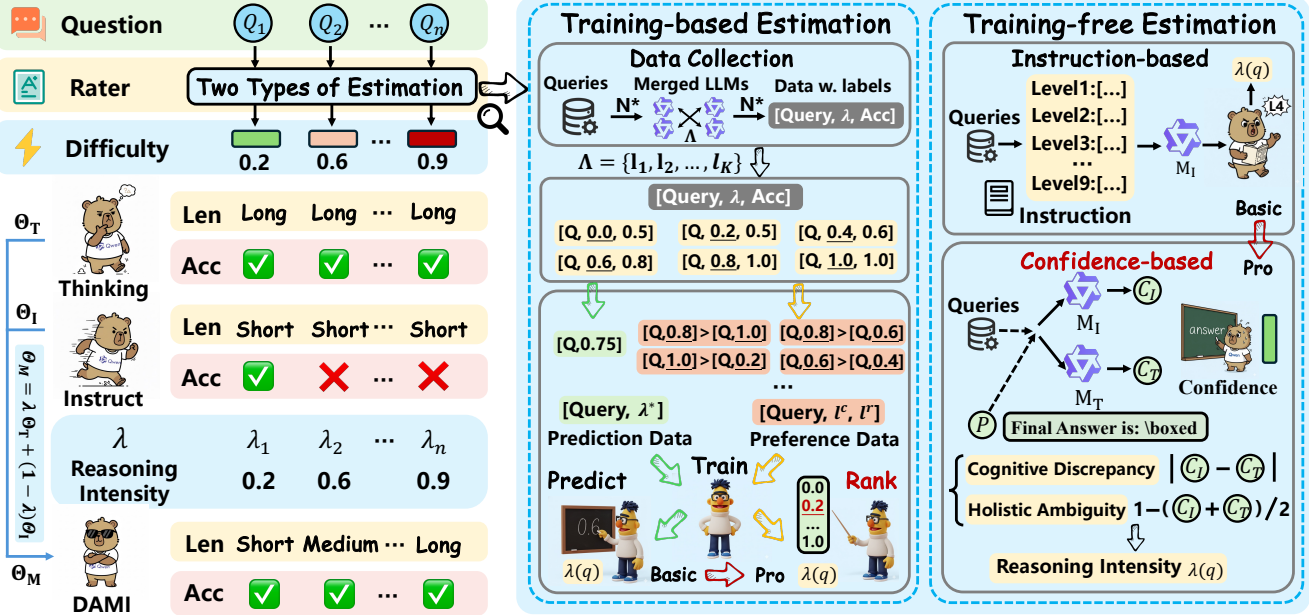


Figure 3: An overview of our DAMI method. DAMI estimates query difficulty through either preference learning (training-based) or confidence signals (training-free), then dynamically adjusts the Reasoning Intensity $\lambda(q)$ to configure cognitive depth accordingly.

Preference Data Construction. We construct policy performance tuples $P(q, l_j) = \langle l_j, \text{Acc}(q, l_j), \text{Cost}(q, l_j) \rangle$, where Cost is the average token count. Preference pairs are generated according to a hierarchical criterion:

$$P_i \succ P_j \iff \begin{cases} \text{Acc}_i > \text{Acc}_j + \delta_{\text{acc}} \\ |\text{Acc}_i - \text{Acc}_j| \leq \delta_{\text{acc}} \wedge \text{Cost}_i < \text{Cost}_j \end{cases} \quad (5)$$

where δ_{acc} is a small tolerance threshold to account for sampling noise. This criterion prioritizes accuracy while using efficiency as a tiebreaker, directly reflecting the practical goal of achieving high performance at minimal cost. Pairs without clear preference are discarded to ensure signal quality. This process is applied to all pairs to construct the final dataset:

$$\mathcal{D}_{\text{pref}} = \{(q, l_c, l_r) \mid P(q, l_c) \succ P(q, l_r)\} \quad (6)$$

Optimization and Inference. The reward model is optimized via binary cross-entropy loss:

$$\mathcal{L}(\psi) = -\mathbb{E}_{(q, l_c, l_r) \sim \mathcal{D}_{\text{pref}}} [\log \sigma (R_\psi(q, l_c) - R_\psi(q, l_r))] \quad (7)$$

3.4 Training-free Estimation of λ

Baseline: Prompt-based Estimation

A straightforward approach is to leverage the model’s in-context learning for difficulty assessment. We design a zero-shot prompt that instructs the Instruct model to rate query difficulty on a scale from 1 to 9 (see Figure 11 in Appendix C), then linearly scale to obtain $\lambda(q)$. However, this method depends heavily on instruction-following capability and generalizes poorly across model families.

DAMI-Conf: Confidence-based Estimation

Considering the above drawbacks, we propose to derive $\lambda(q)$ from intrinsic confidence signals, offering two advantages: model-agnostic signals that generalize across architectures, and continuous-valued output for fine-grained control.

Confidence Extraction. Following Yang *et al.* [2025c], we define confidence as the geometric mean of maximum token probabilities over the answer sequence $\mathbf{a} = (a_1, \dots, a_n)$:

$$\mathcal{C}(\mathcal{M}, q) = \left(\prod_{t=1}^n \max_{a_t \in \mathcal{V}} \text{softmax}(\mathcal{M}(q, i, \mathbf{a}_{<t}))_t \right)^{1/n} \quad (8)$$

where i is an answer-inducing prompt like "Final answer is: \boxed{ }". We compute $\mathcal{C}^I(q)$ and $\mathcal{C}^T(q)$ for the Instruct and Thinking models respectively.

Dual-Signal Fusion. We construct $\lambda(q)$ from two complementary signals that capture different aspects of query difficulty. *Holistic Ambiguity* measures overall system uncertainty. When neither model is confident, the query is likely challenging and requires deeper reasoning:

$$S_{\text{ambi}}(q) = 1 - \frac{\mathcal{C}^I(q) + \mathcal{C}^T(q)}{2} \quad (9)$$

Cognitive Discrepancy quantifies the disagreement between models by measuring the difference in their confidence. A high discrepancy suggests that the two models employ different strategies for addressing the query, indicating potential ambiguity that requires extensive reasoning to resolve:

$$S_{\text{dis}}(q) = |\mathcal{C}^I(q) - \mathcal{C}^T(q)| \quad (10)$$

The fused signal $S_{\text{final}} = S_{\text{ambi}} + S_{\text{dis}}$ is transformed via calibrated sigmoid to yield Reasoning Intensity:

$$\lambda(q) = \sigma \left(\frac{S_{\text{final}}(q) - \mu}{\tau} \right) \quad (11)$$

Method	GSM8K				MATH-500				AMC				AIME24				AIME25				Overall		
	Acc↑ 2×	Tok↓ #N	CR↓ %	Think #R	Acc↑ 2×	Tok↓ #N	CR↓ %	Think	Acc↑ 8×	Tok↓ #N	CR↓ %	Think #R	Acc↑ 8×	Tok↓ #N	CR↓ %	Think #R	Acc↑ 8×	Tok↓ #N	CR↓ %	Think #R	Acc↑ - CR↓ %	Think #R	
Qwen3-4B-2507-Thinking/Qwen3-4B-2507-Instruct																							
Instruct	94.3	349	23.1	0	93.1	1741	26.1	0	93.8	3034	27.4	0	61.7	8938	46.5	0	49.2	8384	39.3	0	78.4	37.5	0
Thinking	95.5	1510	100	100	96.1	6668	100	100	99.4	11076	100	100	78.3	19241	100	100	71.7	21340	100	100	88.2	100	100
DEER	95.5	1059	70	100	95.4	6125	92	100	100	10084	91	100	83.3	18065	94	100	76.7	19287	90	100	90.2	87	100
TA	95	1225	81	100	96.5	4671	70	100	100	7760	70	100	78.3	13515	70	98	73.3	15546	73	98	88.6	73	99
TIES	94	363	24	0	94.8	1899	28	0	95.6	3012	27	0	68.3	8141	42	0	51.7	8419	39	0	80.9	32	0
MI-03	94	383	25	0	95.3	1933	29	0	96.2	3381	31	0	67.5	9708	50	0	51.7	9280	43	0	81	36	0
MI-05	95.1	1084	72	83	96.1	3213	48	72	96.2	5138	46	61	73.3	9321	48	50	65.8	10533	49	54	85.3	53	64
MI-07	95.4	1222	81	100	96.4	4617	69	100	100	7501	68	100	82.5	13993	73	100	75	16086	75	98	89.9	73	100
Routing	94.5	430	28	2.7	96.4	5435	82	53.8	100	10356	93	85	76.7	19861	103	100	73.3	21035	99	100	88.2	81	68.3
DAMI-Pred	94.4	365	24	0	95.6	1886	28	0	95	3477	31	0	73.3	7703	40	0	53.3	8776	41	0	83.3	33	0
DAMI-Prompt	95.5	1028	68	59	95	2832	42	27	95.6	4715	43	30	80	10648	55	76	75	13009	61	88	88.2	54	56
DAMI-Pref	94.5	843	56	25	96.4	4315	65	64	98.8	7872	71	86	85	15412	80	95	83.3	17488	82	92	91.6	71	72
DAMI-Conf	94.5	856	57	41	96.2	2954	44	34	98.8	5891	53	55	85	13485	70	79	79.2	16412	77	94	90.7	60	61
DeepSeek-R1-Distill-Qwen-7B/Qwen2.5-Math-7B																							
Instruct	55.3	1007	-	0	52	1268	-	0	42.5	1463	-	0	20	1470	-	0	3.3	1104	-	0	34.6	-	0
Thinking	89.6	1886	100	100	86	5881	100	100	87.5	8600	100	100	43.3	17887	100	100	30	21681	100	100	67.3	100	100
DEER	89.5	873	46	100	88.8	3140	53	100	82.5	7398	86	100	45	13945	78	100	30	15941	74	100	67.2	67	100
TA	90.7	769	41	99	88.8	2670	45	97	78.1	4319	50	96	39.2	9396	53	92	25.8	11189	52	83	64.5	48	93
TIES	86.5	346	18	0	80.2	827	14	0	58.1	1263	15	0	16.7	1739	10	0	10	1827	8	0	50.3	13	0
MI-03	85.5	379	20	0	76.8	1501	26	0	57.5	1817	21	0	23.3	3459	19	0	16.7	4485	21	0	52	21	0
MI-05	91.9	617	33	71	83.6	2338	40	13	72.5	4462	52	8	20	15330	86	0	20	10665	49	0	57.6	52	18
MI-07	91.2	902	48	99	88.2	3243	55	95	85	4867	57	92	36.7	18693	105	50	30	17169	79	60	66.2	69	79
Routing	64.5	1045	55	0	63.6	1303	22	4.4	50	1425	17	5	25	1875	10	20	6.7	2851	13	10	42	24	7.9
DAMI-Pred	83.5	410	22	0	79.6	1823	31	0	62.5	3103	36	20	26.7	13209	74	31	13.3	13813	64	26	53.1	45	15.4
DAMI-Prompt	82.1	431	23	0	76.2	1657	28	0	55	1697	20	0	20	3962	22	0	10	4962	23	0	48.7	23	0
DAMI-Pref	92.4	1121	59	48	89.4	3952	67	75	88.8	5819	68	88	45	14561	81	92	32.5	16837	78	94	69.6	71	79.4
DAMI-Conf	91.8	1050	56	55	89	3526	60	62	87.5	5299	62	78	44.2	13835	77	85	30	16174	75	90	68.9	66	74

Table 1: Experimental results on two model pairs (Qwen3-4B and Qwen2.5-7B) across five mathematical reasoning benchmarks. "Acc" denotes accuracy, "Tok" denotes token count, "CR" denotes compression rate, and "Think" denotes thinking ratio. ↑/↓ indicate that higher/lower values are better. The top-2 best results are highlighted in **bold**. The result is statistically significant with p -value < 0.05 .

where μ and τ control the decision boundary and sensitivity.

4 Experiments

4.1 Experimental Setup

Models and Datasets. We conduct experiments on the following two pairs of open-source models: (Qwen3-4B-2507-Thinking, Qwen3-4B-2507-Instruct) and (DeepSeek-R1-Distill-Qwen-7B, Qwen2.5-Math-7B). The evaluation benchmarks primarily consist of mathematical reasoning tasks, encompassing five specific datasets ranging from simple to difficult: GSM8K [Cobbe *et al.*, 2021], MATH-500 [Hendrycks *et al.*, 2021], AMC 2023 [AI-MO, 2024], AIME 2024, and AIME 2025 [MAA Committees]. For the training of the router model and reward model, we select training data from DeepMath [He *et al.*, 2025], which is out-of-distribution (OOD) relative to the evaluation sets. Since this dataset inherently contains difficulty labels, we first conduct an initial screening based on these labels, selecting an average of 1,000 samples across various difficulty levels for constructing the training data described in Section 3.2.

Baselines. We compare our methods (DAMI-Pref, DAMI-Conf) against three categories of approaches: (1) **output control methods**, including the early-exit approach DEER [Yang *et al.*, 2025c]; (2) **static capability control methods**, including Task Arithmetic (TA) [Ilharco *et al.*, 2023], TIES-Merging (TIES) [Yadav *et al.*, 2023], and Model Interpolation (MI) [Wu *et al.*, 2025b], which apply fixed merging coefficients across all queries; and (3) **dynamic capability control methods**, including prompt-based LLM Routing, as well as two strong dynamic merging baselines introduced in this work (DAMI-Pred, DAMI-Prompt). We also include the two original models (Instruct, Thinking) as reference endpoints. The hyperparameters for all baseline methods are set strictly according to the original papers.

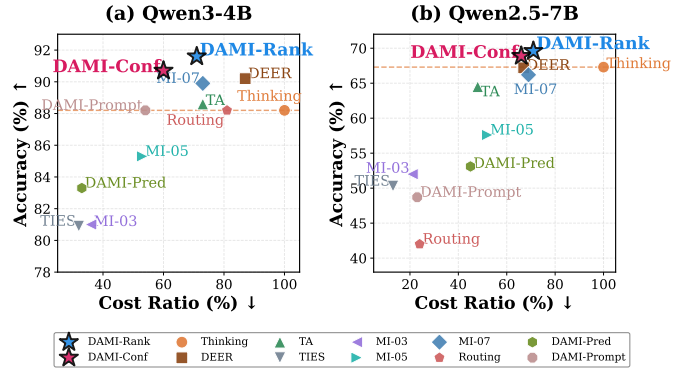


Figure 4: Accuracy-efficiency scatter plot aggregated over five benchmarks. DAMI methods (starred) achieve the best accuracy-efficiency trade-offs on both Qwen3-4B and Qwen2.5-7B.

Metrics and Implementations. We selected Accuracy (Acc $n \times$), Token Number (Tok #N), and Thinking Ratio (Think #R) as our evaluation metrics. Acc $n \times$ denotes the final answer accuracy, and $n \times$ represents the number of sampling rounds conducted for evaluation. Tok #N indicates the aver-

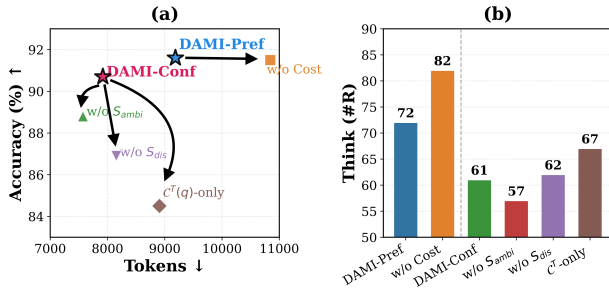


Figure 5: Ablation study results on the Qwen3-4B model pair.

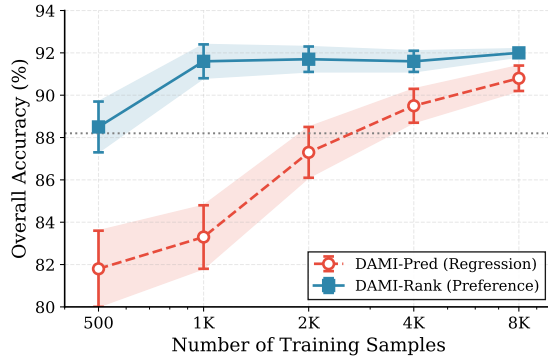


Figure 6: Effect of training data size on training-based λ estimation.

age number of generated tokens per sample, serving as a measure of computational cost. **Think #R** is defined as the percentage of responses containing the $\langle\text{think}\rangle$ token, quantifying the prevalence of explicit CoT reasoning. Given the limited sample sizes in the AMC 2023, AIME 2024, and AIME 2025 datasets, we perform 8 sampling rounds per instance and average the results across all metrics to ensure statistical stability and reliability. Across all models, we consistently apply the hyperparameters $T = 0.6$ and Top-p= 0.95. For confidence-based estimation, we set $\mu = 0.3$ and $\tau = 0.3$.

4.2 Experimental Results

Overall Performance. As shown in Table 1, DAMI-Pref and DAMI-Conf consistently achieve the best performance across both model families. On Qwen3-4B pair, DAMI-Pref attains 91.6% accuracy (+3.4% absolute) while reducing token consumption by 29% compared to vanilla Thinking. DAMI-Conf further improves efficiency with 40% token reduction while maintaining 90.7% accuracy (+2.5% absolute). Figure 4 visualizes the overall accuracy-efficiency trade-off: DAMI-Pref and DAMI-Conf consistently occupy the Pareto-optimal region, dominating both output control methods and static capability control methods across both model pairs.

Comparison of Strong Dynamic Merging Baselines. The DAMI-Pred consistently underestimates required reasoning intensity, achieving only 83.3% accuracy versus 91.6% for DAMI-Pref on Qwen3-4B. The DAMI-Prompt performs reasonably on Qwen3-4B but degrades severely on 7B, as Qwen2.5-Math-7B lacks robust instruction-following for difficulty assessment. In contrast, DAMI-Pref benefits from

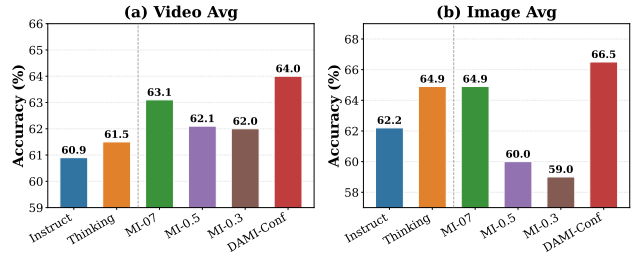


Figure 7: Generalization to multimodal tasks of DAMI.

pairwise comparisons that are robust to label noise, while DAMI-Conf leverages model-agnostic confidence signals that generalize across architectures.

Comparison with SoTA Methods. DEER achieves comparable accuracy to DAMI-Pref on Qwen3-4B but consumes more tokens and risks truncated reasoning. LLM Routing suffers from its discrete nature: on Qwen2.5-7B, it collapses to 42.0% accuracy due to the weak System 1 model, while our continuous interpolation maintains robust performance. Static merging methods (TA, TIES, MI- λ) cannot adapt to varying difficulty distributions. While MI-07 achieves strong results on Qwen3-4B, our dynamic approach consistently outperforms the best static configuration across benchmarks.

Analysis of Thinking Ratio. The Thinking Ratio reveals adaptive resource allocation. On simpler benchmarks like GSM8K, DAMI-Pref and DAMI-Conf activate deep thinking for only 25-41% of queries on Qwen3-4B. As difficulty increases toward AIME24/25, the ratio rises to 79-95%. This adaptive behavior distinguishes our approach from static methods, which either overthink simple queries (Thinking, TA) or underthink difficult ones (TIES, MI-03). The smooth variation demonstrates that DAMI successfully calibrates reasoning depth to query complexity.

4.3 Analysis

Ablation study. Figure 5 presents ablation results on the Qwen3-4B model pair, examining the contribution of key design components. For DAMI-Pref, removing the cost-based tiebreaker (-Cost) slightly improves accuracy but increases token consumption by 18.0%. This confirms that the hierarchical preference criterion effectively balances accuracy and efficiency. For DAMI-Conf, both signals contribute to the final performance. Removing Cognitive Discrepancy (- S_{dis}) causes a 3.7% accuracy drop, while removing Holistic Ambiguity (- S_{ambi}) results in a 1.9% drop. Using only the Thinking model's confidence ($C^T(q)$ -only) degrades accuracy to 84.5%, demonstrating that the inter-model comparison is essential for reliable difficulty estimation. More detailed results are provided in Table 2 (Appendix).

Training data efficiency of DAMI-Pref. Figure 6 compares DAMI-Pred and DAMI-Pref under varying training data sizes. DAMI-Pref achieves near-optimal performance with only 1K samples and shows minimal improvement beyond, demonstrating strong robustness to limited supervision. In contrast, DAMI-Pred requires significantly more data to stabilize: it does not surpass the Thinking baseline until 4K samples. This gap confirms our motivation for preference-based

Question: The volume of the cylinder shown is 45π cubic cm. What is the height in centimeters of the cylinder? [asy]\nsize(120); draw(shift(2,2,0)*scale(0.3)*Circle((0,0), 1.2)); draw((1,0)--(-1,2));\nndraw((3,4.0)--(-3,4,-2));\n\ndraw((1,-2)..(2.2,-2.36)..(3.4,-2));\n\nlabel("\$h\$",(midpoint((3,4.0)--(3.4,-2)),E));\n\nndraw (((2,2,0)--(-3,4,0))); \n\nlabel("\$r=3\$",(midpoint((2,2,0)--(-3,4,0)),N));\n\n[/asy]

Original Response

This is a complex or challenging question, and it is difficult to provide a direct and correct answer. I need to think about it. Well, so I need to find the height of this cylinder. The problem says the volume is 45π cubic cm. **<omitted>** $V = \pi r^2 h$. Solve for h : $h = V / (\pi r^2)$. Plug in $V = 45\pi$, $r = 3$. So $h = (45\pi) / (\pi * 3^2) = (45\pi) / (9\pi) = 45/9 = 5$. Yep, the π cancels, 45 divided by 9 is 5. So height is 5 cm. **Wait, (exit here)**

Is there any chance the diagram is tricking me? **<omitted>** Let me recap to make sure I didn't skip any steps. **<omitted>** **</think>** To find the **height** of a cylinder when given its **volume** and **radius**, **<omitted>** **Final Answer:** $\boxed{5}$.

Token number: 2846

DEER

This is a complex or challenging question, and it is difficult to provide a direct and correct answer. I need to think about it. Well, so I need to find the height of this cylinder. The problem says the volume is 45π cubic cm. **<omitted>** $V = \pi r^2 h$. Solve for h : $h = V / (\pi r^2)$. Plug in $V = 45\pi$, $r = 3$. So $h = (45\pi) / (\pi * 3^2) = (45\pi) / (9\pi) = 45/9 = 5$. Yep, the π cancels, 45 divided by 9 is 5. So height is 5 cm. **Wait, (exit here)**

</think> To determine the height of the cylinder, we begin by recalling the standard formula for the volume of a cylinder: $\pi r^2 h$. Where: π is the volume, **<omitted>** **Final Answer:** $\boxed{5}$.

Token number: 1188

LLM Routing

This is a complex or challenging question and it is difficult to provide a direct and correct answer. I need to think about it. Well, so I need to find the height of a cylinder when they give me the volume and some info about the radius. Let me start by recalling the formula for the volume of a cylinder. Hmm, volume is base area times height, right? And the base of a cylinder is **<omitted>** **Wait, let me make sure I'm not misinterpreting the label.** **<omitted>** Let me confirm once more. **<omitted>** **Wait, hold on,** sometimes people confuse radius and diameter in diagrams. **<omitted>** **</think>** To determine the height of the cylinder **<omitted>** **Final Answer:** $\boxed{5}$.

Token number: 3017

DAMI's (2=0.4)

We are given that the volume of the cylinder is 45π cubic centimeters, and we are to find the height h . The formula for the volume of a cylinder is: $\pi r^2 h$. From the diagram, we are told that the radius $r = 3$ cm. Substitute the known values into the volume formula: $45\pi = \pi r^2 h$. Simplify $45 = 9\pi h$. Divide both sides by 9π : $h = \frac{45}{9\pi} = 5$. Now solve for h : $h = \frac{45}{9\pi} = 5$. **Final Answer:** $\boxed{5}$.

Token number: 351

Figure 8: Comparison of responses generated by four methods. DAMI produces efficient reasoning by modulating cognitive configuration.

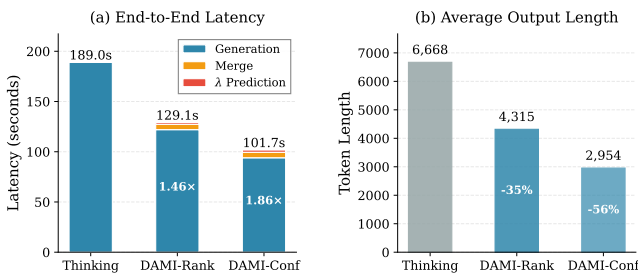


Figure 9: Computational cost analysis on MATH-500 (Qwen3-4B). (a) End-to-end latency breakdown showing λ prediction, parameter merging, and generation time. (b) Average output token length.

estimation: pairwise comparisons provide more robust learning signals than pointwise regression, particularly in low-data regimes where label noise has greater impact.

Case study. Figure 8 compares responses on a geometry problem from MATH-500. The Thinking model produces 2,846 tokens with typical overthinking patterns. DEER reduces output to 1,188 tokens through early termination, but cannot skip the lengthy content before the exit marker. This reflects a fundamental limitation of output control methods. LLM Routing, constrained to discrete model selection, routes this query to Thinking and yields 3,017 tokens. In contrast, DAMI generates only 351 tokens with qualitatively different behavior: direct problem formulation, concise calculation, and no redundant verification. This illustrates the core advantage of capability control: DAMI produces inherently efficient reasoning by modulating cognitive configuration.

Generalization on Multimodal Tasks. Beyond text-only models, we evaluate DAMI on the multimodal model Qwen3-VL-8B [Bai *et al.*, 2025]. We curate a diverse evaluation suite comprising 5 video understanding benchmarks (Video-Holmes, MMVU, VideoMMU, VideoMME, LVbench) and 4 image-text reasoning benchmarks (WeMath, Math-Vista, MMMU, MathVision). As shown in Figure 7, DAMI-Conf consistently outperforms all baselines across both modalities. On video understanding tasks, DAMI-Conf

achieves 64.0% average accuracy, surpassing the Thinking model by 2.5% absolute. On image-text reasoning tasks, DAMI-Conf attains 66.5%, a 1.6% improvement over Thinking. These findings confirm that our DAMI framework generalizes effectively to widely multimodal tasks. Moreover, it reveals that DAMI not only enables efficient reasoning, but also effectively integrates the complementary knowledge and reasoning capabilities of both models, leading to consistent performance gains across diverse benchmarks.

Computational cost. Figure 9 presents end-to-end latency. Despite introducing additional steps for λ prediction and parameter merging, both methods achieve substantial speedups over vanilla Thinking. The overhead from λ prediction is modest: DAMI-Pref only requires scoring each candidate λ with a lightweight reward model, while DAMI-Conf extracts confidence from short answer-only generations rather than full reasoning chains. Parameter merging adds ~ 5.3 s when loading models on-demand, but this can be reduced to under 1s by pre-loading both checkpoints into GPU memory. These overheads are negligible compared to generation time, which dominates total latency. By reducing output length by 35% (DAMI-Pref) and 56% (DAMI-Conf), our methods achieve 1.46 \times and 1.86 \times end-to-end speedups respectively.

5 Conclusion

This paper addresses the challenge that System 1’s efficiency and System 2’s reasoning capability cannot be readily unified within a single model. Unlike existing methods that constrain what models produce (output control), we propose capability control, which modulates how models think through dynamic parameter interpolation. Our DAMI framework offers two complementary methods, training based DAMI-Pref and training free DAMI-Conf, to achieve query-adaptive reasoning intensity. Beyond the technical contributions, this work suggests a broader perspective: the dichotomy between fast and slow thinking need not be a binary choice resolved at training time. The monotonicity and continuity properties we establish indicate that reasoning depth exists on a smooth spectrum, accessible through simple linear operations in parameter space. This finding opens possibilities for more flex-

ible cognitive architectures that adapt computational budget.

References

AI-MO. Amc 2023, 2024.

Yash Akhauri, Anthony Fei, Chi-Chih Chang, Ahmed F. AbouElhamayed, Yueying Li, and Mohamed S. Abdelfattah. Splitreason: Learning to offload reasoning, 2025.

Daman Arora and Andrea Zanette. Training language models to reason efficiently, 2025.

Shuai Bai, Yuxuan Cai, Ruizhe Chen, Keqin Chen, Xionghui Chen, Zesen Cheng, Lianghao Deng, Wei Ding, Chang Gao, Chunjiang Ge, Wenbin Ge, Zhifang Guo, Qidong Huang, Jie Huang, Fei Huang, Binyuan Hui, Shutong Jiang, Zhaohai Li, Mingsheng Li, Mei Li, Kaixin Li, Zicheng Lin, Junyang Lin, Xuejing Liu, Jiawei Liu, Chenglong Liu, Yang Liu, Dayiheng Liu, Shixuan Liu, Dunjie Lu, Ruilin Luo, Chenxu Lv, Rui Men, Lingchen Meng, Xuancheng Ren, Xingzhang Ren, Sibo Song, Yuchong Sun, Jun Tang, Jianhong Tu, Jianqiang Wan, Peng Wang, Pengfei Wang, Qiuyue Wang, Yuxuan Wang, Tianbao Xie, Yiheng Xu, Haiyang Xu, Jin Xu, Zhibo Yang, Mingkun Yang, Jianxin Yang, An Yang, Bowen Yu, Fei Zhang, Hang Zhang, Xi Zhang, Bo Zheng, Humen Zhong, Jingren Zhou, Fan Zhou, Jing Zhou, Yuanzhi Zhu, and Ke Zhu. Qwen3-vl technical report. *arXiv preprint arXiv:2511.21631*, 2025.

Siyuan Chen, Qingyi Si, Chenxu Yang, Yunzhi Liang, Zheng Lin, Huan Liu, and Weiping Wang. A multi-task role-playing agent capable of imitating character linguistic styles, 2024.

Karl Cobbe, Vineet Kosaraju, Mohammad Bavarian, Mark Chen, Heewoo Jun, Lukasz Kaiser, Matthias Plappert, Jerry Tworek, Jacob Hilton, Reiichiro Nakano, Christopher Hesse, and John Schulman. Training verifiers to solve math word problems, 2021.

Muzhi Dai, Chenxu Yang, and Qingyi Si. S-grpo: Early exit via reinforcement learning in reasoning models, 2025.

DeepSeek-AI, Daya Guo, Dejian Yang, Haowei Zhang, Junxiao Song, Ruoyu Zhang, Runxin Xu, Qihao Zhu, Shirong Ma, Peiyi Wang, Xiao Bi, Xiaokang Zhang, Xingkai Yu, Yu Wu, Z. F. Wu, Zhibin Gou, Zhihong Shao, Zhuoshu Li, Ziyi Gao, Aixin Liu, Bing Xue, Bingxuan Wang, Bochao Wu, Bei Feng, Chengda Lu, Chenggang Zhao, Chengqi Deng, Chenyu Zhang, Chong Ruan, Damai Dai, Deli Chen, Dongjie Ji, Erhang Li, Fangyun Lin, Fucong Dai, Fuli Luo, Guangbo Hao, Guanting Chen, Guowei Li, H. Zhang, Han Bao, Hanwei Xu, Haocheng Wang, Honghui Ding, Huajian Xin, Huazuo Gao, Hui Qu, Hui Li, Jianzhong Guo, Jiashi Li, Jiawei Wang, Jingchang Chen, Jingyang Yuan, Junjie Qiu, Junlong Li, J. L. Cai, Jiaqi Ni, Jian Liang, Jin Chen, Kai Dong, Kai Hu, Kaige Gao, Kang Guan, Kexin Huang, Kuai Yu, Lean Wang, Lecong Zhang, Liang Zhao, Litong Wang, Liyue Zhang, Lei Xu, Leyi Xia, Mingchuan Zhang, Minghua Zhang, Minghui Tang, Meng Li, Miaojun Wang, Mingming Li, Ning Tian, Panpan Huang, Peng Zhang, Qiancheng Wang, Qinyu Chen, Qiushi Du, Ruiqi Ge, Ruisong Zhang, Ruizhe Pan, Runji

Wang, R. J. Chen, R. L. Jin, Ruyi Chen, Shanghao Lu, Shangyan Zhou, Shanhua Chen, Shengfeng Ye, Shiyu Wang, Shuiping Yu, Shunfeng Zhou, Shuting Pan, S. S. Li, Shuang Zhou, Shaoqing Wu, Shengfeng Ye, Tao Yun, Tian Pei, Tianyu Sun, T. Wang, Wangding Zeng, Wanjia Zhao, Wen Liu, Wenfeng Liang, Wenjun Gao, Wenqin Yu, Wentao Zhang, W. L. Xiao, Wei An, Xiaodong Liu, Xiaohan Wang, Xiaokang Chen, Xiaotao Nie, Xin Cheng, Xin Liu, Xin Xie, Xingchao Liu, Xinyu Yang, Xinyuan Li, Xuecheng Su, Xuheng Lin, X. Q. Li, Xiangyue Jin, Xiaojin Shen, Xiaosha Chen, Xiaowen Sun, Xiaoxiang Wang, Xinnan Song, Xinyi Zhou, Xianzu Wang, Xinxia Shan, Y. K. Li, Y. Q. Wang, Y. X. Wei, Yang Zhang, Yanhong Xu, Yao Li, Yao Zhao, Yaofeng Sun, Yaohui Wang, Yi Yu, Yichao Zhang, Yifan Shi, Yiliang Xiong, Ying He, Yishi Piao, Yisong Wang, Yixuan Tan, Yiyang Ma, Yiyuan Liu, Yongqiang Guo, Yuan Ou, Yuduan Wang, Yue Gong, Yuheng Zou, Yujia He, Yunfan Xiong, Yuxiang Luo, Yuxiang You, Yuxuan Liu, Yuyang Zhou, Y. X. Zhu, Yanhong Xu, Yanping Huang, Yaohui Li, Yi Zheng, Yuchen Zhu, Yunxian Ma, Ying Tang, Yukun Zha, Yuting Yan, Z. Z. Ren, Zehui Ren, Zhangli Sha, Zhe Fu, Zhean Xu, Zhenda Xie, Zhengyan Zhang, Zhewen Hao, Zhicheng Ma, Zhi-gang Yan, Zhiyu Wu, Zihui Gu, Zijia Zhu, Zijun Liu, Zilin Li, Ziwei Xie, Ziyang Song, Zizheng Pan, Zhen Huang, Zhipeng Xu, Zhongyu Zhang, and Zhen Zhang. Deepseek-r1: Incentivizing reasoning capability in llms via reinforcement learning, 2025.

Siqi Fan, Bowen Qin, Peng Han, Shuo Shang, Yequan Wang, and Aixin Sun. The price of a second thought: On the evaluation of reasoning efficiency in large language models, 2025.

Jonathan Frankle, Gintare Karolina Dziugaite, Daniel M. Roy, and Michael Carbin. Linear mode connectivity and the lottery ticket hypothesis, 2020.

Tingxu Han, Zhenting Wang, Chunrong Fang, Shiyu Zhao, Shiqing Ma, and Zhenyu Chen. Token-budget-aware LLM reasoning. In Wanxiang Che, Joyce Nabende, Ekaterina Shutova, and Mohammad Taher Pilehvar, editors, *Findings of the Association for Computational Linguistics: ACL 2025*, pages 24842–24855, Vienna, Austria, July 2025. Association for Computational Linguistics.

Zhiwei He, Tian Liang, Jiahao Xu, Qiuwei Liu, Xingyu Chen, Yue Wang, Linfeng Song, Dian Yu, Zhenwen Liang, Wenxuan Wang, Zhuseng Zhang, Rui Wang, Zhaopeng Tu, Haitao Mi, and Dong Yu. Deepmath-103k: A large-scale, challenging, decontaminated, and verifiable mathematical dataset for advancing reasoning, 2025.

Dan Hendrycks, Collin Burns, Saurav Kadavath, Akul Arora, Steven Basart, Eric Tang, Dawn Song, and Jacob Steinhardt. Measuring mathematical problem solving with the math dataset, 2021.

Bairu Hou, Yang Zhang, Jiabao Ji, Yujian Liu, Kaizhi Qian, Jacob Andreas, and Shiyu Chang. Thinkprune: Pruning long chain-of-thought of llms via reinforcement learning, 2025.

Gabriel Ilharco, Marco Tilio Ribeiro, Mitchell Wortsman, Suchin Gururangan, Ludwig Schmidt, Hannaneh Hajishirzi, and Ali Farhadi. Editing models with task arithmetic, 2023.

Zhong-Zhi Li, Duzhen Zhang, Ming-Liang Zhang, Jiaxin Zhang, Zengyan Liu, Yuxuan Yao, Haotian Xu, Junhao Zheng, Pei-Jie Wang, Xiuyi Chen, Yingying Zhang, Fei Yin, Jiahua Dong, Zhiwei Li, Bao-Long Bi, Ling-Rui Mei, Junfeng Fang, Xiao Liang, Zhijiang Guo, Le Song, and Cheng-Lin Liu. From system 1 to system 2: A survey of reasoning large language models, 2025.

Haotian Luo, Haiying He, Yibo Wang, Jinluan Yang, Rui Liu, Naiqiang Tan, Xiaochun Cao, Dacheng Tao, and Li Shen. Ada-r1: Hybrid-cot via bi-level adaptive reasoning optimization, 2025.

MAA Committees. Aime problems and solutions. https://artofproblemsolving.com/wiki/index.php/AIME_Problems_and_Solutions.

Behnam Neyshabur, Hanie Sedghi, and Chiyuan Zhang. What is being transferred in transfer learning? In *Advances in Neural Information Processing Systems*, volume 33, pages 512–523, 2020.

Isaac Ong, Amjad Almahairi, Vincent Wu, Wei-Lin Chiang, Tianhao Wu, Joseph E. Gonzalez, M Waleed Kadous, and Ion Stoica. Routellm: Learning to route llms with preference data, 2025.

OpenAI. Learning to reason with llms, September 2024.

Raphael Schumann, Elman Mansimov, Yi-An Lai, Nikolaos Pappas, Xibin Gao, and Yi Zhang. Backward compatibility during data updates by weight interpolation, 2023.

Yi Shen, Jian Zhang, Jieyun Huang, Shuming Shi, Wenjing Zhang, Jiangze Yan, Ning Wang, Kai Wang, Zhaoxiang Liu, and Shiguo Lian. Dast: Difficulty-adaptive slow-thinking for large reasoning models, 2025.

Mustafa Shukor, Louis Bethune, Dan Busbridge, David Grangier, Enrico Fini, Alaaeldin El-Nouby, and Pierre Ablin. Scaling laws for optimal data mixtures, 2025.

Jinyan Su and Claire Cardie. Thinking fast and right: Balancing accuracy and reasoning length with adaptive rewards, 2025.

Kimi Team, Angang Du, Bofei Gao, Bowei Xing, Changjiu Jiang, Cheng Chen, Cheng Li, Chenjun Xiao, Chenzhuang Du, Chonghua Liao, Chunling Tang, Congcong Wang, Dehao Zhang, Enming Yuan, Enzhe Lu, Fengxiang Tang, Flood Sung, Guangda Wei, Guokun Lai, Haiqing Guo, Han Zhu, Hao Ding, Hao Hu, Hao Yang, Hao Zhang, Haotian Yao, Haotian Zhao, Haoyu Lu, Haoze Li, Haozhen Yu, Hongcheng Gao, Huabin Zheng, Huan Yuan, Jia Chen, Jianhang Guo, Jianlin Su, Jianzhou Wang, Jie Zhao, Jin Zhang, Jingyuan Liu, Junjie Yan, Junyan Wu, Lidong Shi, Ling Ye, Longhui Yu, Mengnan Dong, Neo Zhang, Ningchen Ma, Qiwei Pan, Qucheng Gong, Shaowei Liu, Shengling Ma, Shupeng Wei, Sihan Cao, Siying Huang, Tao Jiang, Weihao Gao, Weimin Xiong, Weiran He, Weixiao Huang, Weixin Xu, Wenhao Wu, Wenyang He, Xianhui Wei, Xianqing Jia, Xingzhe Wu, Xinran Xu, Xinxing Zu, Xinyu Zhou, Xuehai Pan, Y. Charles, Yang Li, Yangyang Hu, Yangyang Liu, Yanru Chen, Yejie Wang, Yibo Liu, Yidao Qin, Yifeng Liu, Ying Yang, Yiping Bao, Yulun Du, Yuxin Wu, Yuzhi Wang, Zaida Zhou, Zhaoji Wang, Zhaowei Li, Zhen Zhu, Zheng Zhang, Zhexu Wang, Zhilin Yang, Zhiqi Huang, Zihao Huang, Ziying Xu, Zonghan Yang, and Zongyu Lin. Kimi k1.5: Scaling reinforcement learning with llms, 2025.

Qwen Team. Qwen3 technical report, 2025.

Hongyi Wang, Mikhail Yurochkin, Yuekai Sun, Dimitris Pavliopoulos, and Yasaman Khazaeni. Federated learning with matched averaging, 2020.

Lanrui Wang, Jiangnan Li, Chenxu Yang, Zheng Lin, and Weiping Wang. Enhancing empathetic and emotion support dialogue generation with prophetic commonsense inference. *CoRR*, abs/2311.15316, 2023.

Han Wu, Yuxuan Yao, Shuqi Liu, Zehua Liu, Xiaojin Fu, Xiongwei Han, Xing Li, Hui-Ling Zhen, Tao Zhong, and Mingxuan Yuan. Unlocking efficient long-to-short llm reasoning with model merging, 2025.

Taiqiang Wu, Runming Yang, Tao Liu, Jiahao Wang, and Ngai Wong. Revisiting model interpolation for efficient reasoning, 2025.

Heming Xia, Chak Tou Leong, Wenjie Wang, Yongqi Li, and Wenjie Li. Tokenskip: Controllable chain-of-thought compression in llms, 2025.

Prateek Yadav, Derek Tam, Leshem Choshen, Colin Raffel, and Mohit Bansal. Ties-merging: Resolving interference when merging models, 2023.

Chenxu Yang, Zheng Lin, Lanrui Wang, Chong Tian, Liang Pang, Jiangnan Li, Qirong Ho, Yanan Cao, and Weiping Wang. Multi-level adaptive contrastive learning for knowledge internalization in dialogue generation, 2023.

Enneng Yang, Zhenyi Wang, Li Shen, Shiwei Liu, Guibing Guo, Xingwei Wang, and Dacheng Tao. Adamerging: Adaptive model merging for multi-task learning, 2024.

Chenxu Yang, Ruipeng Jia, Mingyu Zheng, Naibin Gu, Zheng Lin, Siyuan Chen, Weichong Yin, Hua Wu, and Weiping Wang. Weights-rotated preference optimization for large language models. In Christos Christodoulopoulos, Tanmoy Chakraborty, Carolyn Rose, and Violet Peng, editors, *Proceedings of the 2025 Conference on Empirical Methods in Natural Language Processing*, pages 26152–26175, Suzhou, China, November 2025. Association for Computational Linguistics.

Chenxu Yang, Qingyi Si, Mz Dai, Dingyu Yao, Mingyu Zheng, Minghui Chen, Zheng Lin, and Weiping Wang. Test-time prompt intervention, 2025.

Chenxu Yang, Qingyi Si, Yongjie Duan, Zheliang Zhu, Chenyu Zhu, Qiaowei Li, Minghui Chen, Zheng Lin, and Weiping Wang. Dynamic early exit in reasoning models, 2025.

Chenxu Yang, Qingyi Si, and Zheng Lin. Breaking the trade-off between faithfulness and expressiveness for large language models, 2025.

Dingyu Yao, Chenxu Yang, Zhengyang Tong, Zheng Lin, Wei Liu, Jian Luan, and Weiping Wang. Vecinfer: Efficient llm inference with low-bit kv cache via outlier-suppressed vector quantization, 2025.

Yuxuan Yao, Shuqi Liu, Zehua Liu, Qintong Li, Mingyang Liu, Xiongwei Han, Zhijiang Guo, Han Wu, and Linqi Song. Activation-guided consensus merging for large language models, 2025.

Keyao Zhan, Puheng Li, and Lei Wu. Analyzing the role of permutation invariance in linear mode connectivity, 2025.

Haozhen Zhang, Tao Feng, and Jiaxuan You. Router-r1: Teaching llms multi-round routing and aggregation via reinforcement learning, 2025.

A Theoretical Analysis

In this appendix, we provide theoretical justifications for the three empirical findings in Section 3.1. We establish that (1) linear interpolation between models satisfying Linear Mode Connectivity does not cross loss barriers, (2) performance monotonicity holds under mild assumptions about capability ordering and interpolation linearity, and (3) representation continuity follows from the Lipschitz properties of transformer networks.

A.1 Interpolation Validity under Linear Mode Connectivity

We establish why linear parameter interpolation between the Instruct and Thinking models yields valid, well-behaved models rather than degenerate solutions.

Theoretical Background

Neural network loss landscapes are highly non-convex, containing multiple local minima separated by regions of high loss. When linearly interpolating between two model parameters, a natural concern is whether the interpolation path crosses such high-loss regions, resulting in degenerate intermediate models [Yao *et al.*, 2025a; Yang *et al.*, 2023].

Definition 1 (Loss Barrier). *Given two parameter configurations $\Theta^{(1)}$ and $\Theta^{(2)}$, a loss barrier of height ϵ exists on the linear path between them if:*

$$\max_{\lambda \in [0, 1]} \mathcal{L}(\Theta_\lambda) > \max\{\mathcal{L}(\Theta^{(1)}), \mathcal{L}(\Theta^{(2)})\} + \epsilon \quad (12)$$

where $\Theta_\lambda = \lambda\Theta^{(2)} + (1 - \lambda)\Theta^{(1)}$ and $\mathcal{L}(\cdot)$ denotes the task loss.

Definition 2 (Linear Mode Connectivity). *Two models $\Theta^{(1)}$ and $\Theta^{(2)}$ satisfy Linear Mode Connectivity (LMC) if no significant loss barrier exists on the linear path between them, i.e., for all $\lambda \in [0, 1]$:*

$$\mathcal{L}(\Theta_\lambda) \leq \max\{\mathcal{L}(\Theta^{(1)}), \mathcal{L}(\Theta^{(2)})\} + \epsilon \quad (13)$$

where ϵ is a small tolerance threshold.

The concept of Linear Mode Connectivity was formally introduced by Frankle *et al.* [2020], who investigated conditions under which neural networks trained with different random seeds remain linearly connected in parameter space [Chen *et al.*, 2024; Yang *et al.*, 2025d].

Existing Theoretical Results

A crucial result for our work comes from Neyshabur *et al.* [2020], who studied the properties of models fine-tuned from pre-trained checkpoints:

Theorem 1 (Same-Basin Property of Fine-tuned Models, Neyshabur *et al.* 2020). *Let $\Theta^{(0)}$ be a pre-trained model, and let $\Theta^{(1)}, \Theta^{(2)}$ be obtained by fine-tuning $\Theta^{(0)}$ on (possibly different) downstream tasks or with different hyperparameters. Then:*

1. *Both $\Theta^{(1)}$ and $\Theta^{(2)}$ remain in the same basin of the loss landscape as $\Theta^{(0)}$.*
2. *The two fine-tuned models are close in parameter space and similar in feature space.*

This theorem has an important implication for linear interpolation:

Corollary 1 (LMC for Co-originated Models). *If $\Theta^{(1)}$ and $\Theta^{(2)}$ are both fine-tuned from the same pre-trained checkpoint $\Theta^{(0)}$, then they satisfy Linear Mode Connectivity.*

Proof. By Theorem 1, both $\Theta^{(1)}$ and $\Theta^{(2)}$ reside in the same optimization basin \mathcal{B} containing $\Theta^{(0)}$. Since an optimization basin is a connected region of low loss, and both endpoints lie within \mathcal{B} , the linear path between them does not exit \mathcal{B} (assuming \mathcal{B} is approximately convex in the local neighborhood). Therefore, no significant loss barrier exists along the interpolation path, satisfying the definition of LMC. \square

Application to Our Setting

We now apply these theoretical results to our specific context.

Proposition 1 (Interpolation Validity for Instruct-Thinking Pairs). *Let $\Theta^{(I)}$ (Instruct) and $\Theta^{(T)}$ (Thinking) be two models derived from the same base pre-trained model through different post-training procedures (instruction tuning and reasoning enhancement, respectively). Then for any $\lambda \in [0, 1]$, the interpolated model $\Theta_\lambda^{(M)} = \lambda\Theta^{(T)} + (1 - \lambda)\Theta^{(I)}$ satisfies:*

$$\mathcal{L}(\Theta_\lambda^{(M)}) \leq \max\{\mathcal{L}(\Theta^{(I)}), \mathcal{L}(\Theta^{(T)})\} + \epsilon \quad (14)$$

Proof. The Instruct and Thinking models in modern LLM families (e.g., Qwen, DeepSeek) are typically produced through the following pipeline:

1. A base model $\Theta^{(0)}$ is pre-trained on large-scale text corpora.
2. The Instruct model $\Theta^{(I)}$ is obtained by fine-tuning $\Theta^{(0)}$ with instruction-following data.
3. The Thinking model $\Theta^{(T)}$ is obtained by further training (from $\Theta^{(0)}$ or $\Theta^{(I)}$) with reasoning-enhanced data and reinforcement learning.

In either case, both models originate from the same pre-trained checkpoint $\Theta^{(0)}$. By Theorem 1 and Corollary 1, they satisfy LMC, which directly implies the bounded loss property. \square

A.2 Sufficient Conditions for Performance Monotonicity

We establish theoretical conditions under which increasing the reasoning intensity λ leads to monotonically improving accuracy.

Assumption 1 (Capability Ordering). *For any query q from the task distribution \mathcal{Q} , let $p^{(I)}(q) \in [0, 1]$ and $p^{(T)}(q) \in [0, 1]$ denote the probability of correctly answering q by the Instruct and Thinking models respectively. We assume:*

$$p^{(T)}(q) \geq p^{(I)}(q), \quad \forall q \in \mathcal{Q} \quad (15)$$

Remark 1. *This assumption reflects the empirical observation that System 2 (Thinking) models, equipped with extended chain-of-thought reasoning, generally achieve higher or equal accuracy compared to System 1 (Instruct) models on reasoning tasks. The assumption allows equality for simple queries where both models succeed.*

Assumption 2 (Bounded Interpolation Deviation). *The success probability of the interpolated model deviates from linear interpolation by a bounded amount:*

$$p_\lambda^{(M)}(q) = \lambda \cdot p^{(T)}(q) + (1 - \lambda) \cdot p^{(I)}(q) + \delta_\lambda(q) \quad (16)$$

where the deviation term $\delta_\lambda(q)$ satisfies:

1. **Boundedness:** $|\delta_\lambda(q)| \leq \delta_{\max}$ for all $\lambda \in [0, 1]$
2. **Lipschitz continuity:** $|\delta_\lambda(q) - \delta_{\lambda'}(q)| \leq L_\delta \cdot |\lambda - \lambda'|$ for all $\lambda, \lambda' \in [0, 1]$

Remark 2. *The Lipschitz condition ensures that the deviation from linearity changes smoothly with λ . This is justified by the representation continuity established in Section A.3: since model representations change smoothly with λ , the resulting success probabilities should also change smoothly.*

Theorem 2 (Monotonicity of Expected Accuracy). *Under Assumptions 1 and 2, if $L_\delta < \mathbb{E}_{q \sim \mathcal{Q}}[p^{(T)}(q) - p^{(I)}(q)]$, then the expected accuracy is monotonically non-decreasing in λ :*

$$\frac{\partial}{\partial \lambda} \mathbb{E}_{q \sim \mathcal{Q}}[p_\lambda^{(M)}(q)] \geq 0 \quad (17)$$

Proof. By Assumption 2, the success probability can be decomposed as:

$$p_\lambda^{(M)}(q) = \lambda \cdot p^{(T)}(q) + (1 - \lambda) \cdot p^{(I)}(q) + \delta_\lambda(q) \quad (18)$$

Taking the derivative with respect to λ :

$$\frac{\partial}{\partial \lambda} p_\lambda^{(M)}(q) = p^{(T)}(q) - p^{(I)}(q) + \frac{\partial \delta_\lambda(q)}{\partial \lambda} \quad (19)$$

By the Lipschitz condition in Assumption 2, where $\delta_\lambda(q)$ is L_δ -Lipschitz in λ , we have:

$$\left| \frac{\partial \delta_\lambda(q)}{\partial \lambda} \right| \leq L_\delta \quad (20)$$

Taking expectation over $q \sim \mathcal{Q}$:

$$\frac{\partial}{\partial \lambda} \mathbb{E}_q[p_\lambda^{(M)}(q)] = \mathbb{E}_q \left[p^{(T)}(q) - p^{(I)}(q) + \frac{\partial \delta_\lambda(q)}{\partial \lambda} \right] \quad (21)$$

$$\geq \mathbb{E}_q[p^{(T)}(q) - p^{(I)}(q)] - L_\delta \quad (22)$$

Under the condition $L_\delta < \mathbb{E}_q[p^{(T)}(q) - p^{(I)}(q)]$:

$$\frac{\partial}{\partial \lambda} \mathbb{E}_q[p_\lambda^{(M)}(q)] \geq \mathbb{E}_q[p^{(T)}(q) - p^{(I)}(q)] - L_\delta > 0 \quad (23)$$

\square

Corollary 2 (Exact Monotonicity under Linear Interpolation). *If the interpolation is exactly linear, i.e., $\delta_\lambda(q) = 0$ for all λ and q , then:*

$$\frac{\partial}{\partial \lambda} p_\lambda^{(M)}(q) = p^{(T)}(q) - p^{(I)}(q) \geq 0 \quad (24)$$

with strict inequality when $p^{(T)}(q) > p^{(I)}(q)$.

Proof. Setting $\delta_\lambda(q) = 0$ in the general formula yields $\frac{\partial}{\partial \lambda} p_\lambda^{(M)}(q) = p^{(T)}(q) - p^{(I)}(q)$, which is non-negative by Assumption 1. \square

Direct Verification of Monotonicity. Figure 2(a) provides direct evidence: accuracy increases monotonically with λ , consistent with the prediction of Theorem 2.

A.3 Representation Continuity via Lipschitz Analysis

We explain why interpolation induces continuous trajectories in representation space, as observed in Figure 2(b). The key insight is that transformer networks are Lipschitz continuous with respect to their parameters.

Definition 3 (Lipschitz Continuity). A function $f : \mathcal{X} \rightarrow \mathcal{Y}$ is L -Lipschitz if for all $x_1, x_2 \in \mathcal{X}$:

$$\|f(x_1) - f(x_2)\| \leq L \cdot \|x_1 - x_2\| \quad (25)$$

For a parametric function $f(x; \theta)$, we distinguish two types of Lipschitz continuity:

- **Input-Lipschitz:** $\|f(x_1; \theta) - f(x_2; \theta)\| \leq L^{(x)} \|x_1 - x_2\|$
- **Parameter-Lipschitz:** $\|f(x; \theta_1) - f(x; \theta_2)\| \leq L^{(\theta)} \|x\| \cdot \|\theta_1 - \theta_2\|$

Lipschitz Properties of Transformer Components

Lemma 1 (Linear Layer). For a linear transformation $f(x; W) = Wx$:

1. Input-Lipschitz with $L^{(x)} = \|W\|$ (spectral norm)
2. Parameter-Lipschitz: $\|W_1x - W_2x\| \leq \|x\| \cdot \|W_1 - W_2\|$

Proof. For input-Lipschitz: $\|Wx_1 - Wx_2\| = \|W(x_1 - x_2)\| \leq \|W\| \cdot \|x_1 - x_2\|$.

For parameter-Lipschitz: $\|W_1x - W_2x\| = \|(W_1 - W_2)x\| \leq \|W_1 - W_2\| \cdot \|x\|$. \square

Lemma 2 (Activation Functions). Common activation functions are Lipschitz continuous:

- ReLU: 1-Lipschitz
- GeLU: approximately 1.13-Lipschitz
- Softmax: 1-Lipschitz (with respect to ℓ_1 norm)

Lemma 3 (Transformer Layer). A transformer layer $f_l(h; \theta_l)$ consisting of multi-head attention and feed-forward sublayers satisfies:

1. Input-Lipschitz with constant $L_l^{(h)}$
2. Parameter-Lipschitz: for bounded input $\|h\| \leq B$,

$$\|f_l(h; \theta_{l,1}) - f_l(h; \theta_{l,2})\| \leq L_l^{(\theta)} \cdot B \cdot \|\theta_{l,1} - \theta_{l,2}\| \quad (26)$$

where $L_l^{(h)}$ and $L_l^{(\theta)}$ depend on the layer architecture and weight magnitudes.

Proof Sketch. The transformer layer is a composition of linear transformations, attention mechanisms, and activation functions. By the chain rule for Lipschitz functions (composition of L_1 -Lipschitz and L_2 -Lipschitz functions is $L_1 L_2$ -Lipschitz), and noting that each component is Lipschitz (Lemmas 1 and 2), the overall layer inherits Lipschitz continuity with respect to both inputs and parameters. \square

Theorem 3 (Representation Continuity). Let $h_\lambda^{(L)}(x)$ denote the final-layer representation of input x under the interpolated model $\Theta_\lambda^{(M)}$. Assume that intermediate representations are bounded: $\|h_\lambda^{(l)}(x)\| \leq B$ for all l and λ . Then there exists a constant $C > 0$ such that for any $\lambda, \lambda' \in [0, 1]$:

$$\|h_\lambda^{(L)}(x) - h_{\lambda'}^{(L)}(x)\| \leq C \cdot |\lambda - \lambda'| \quad (27)$$

That is, the representation is Lipschitz continuous with respect to the interpolation coefficient λ .

Proof. We proceed by analyzing the layer-wise propagation of differences.

Step 1: Parameter Difference. For the interpolated model, the parameters at layer l are:

$$\theta_{l,\lambda} = \lambda \theta_l^{(T)} + (1 - \lambda) \theta_l^{(I)} \quad (28)$$

The parameter difference between two interpolation coefficients is:

$$\|\theta_{l,\lambda} - \theta_{l,\lambda'}\| = |\lambda - \lambda'| \cdot \|\theta_l^{(T)} - \theta_l^{(I)}\| \quad (29)$$

Let $\Delta_l = \|\theta_l^{(T)} - \theta_l^{(I)}\|$ denote the parameter distance at layer l .

Step 2: Layer-wise Recursion. Let $D_l = \|h_\lambda^{(l)}(x) - h_{\lambda'}^{(l)}(x)\|$ denote the representation difference at layer l . Using the triangle inequality:

$$D_l = \|f_l(h_\lambda^{(l-1)}; \theta_{l,\lambda}) - f_l(h_{\lambda'}^{(l-1)}; \theta_{l,\lambda'})\| \quad (30)$$

$$\leq \underbrace{\|f_l(h_\lambda^{(l-1)}; \theta_{l,\lambda}) - f_l(h_\lambda^{(l-1)}; \theta_{l,\lambda'})\|}_{\text{(A): parameter difference}}$$

$$+ \underbrace{\|f_l(h_\lambda^{(l-1)}; \theta_{l,\lambda'}) - f_l(h_{\lambda'}^{(l-1)}; \theta_{l,\lambda'})\|}_{\text{(B): input difference}} \quad (32)$$

By Lemma 3:

- Term (A) $\leq L_l^{(\theta)} \cdot B \cdot \|\theta_{l,\lambda} - \theta_{l,\lambda'}\| = L_l^{(\theta)} \cdot B \cdot |\lambda - \lambda'| \cdot \Delta_l$
- Term (B) $\leq L_l^{(h)} \cdot D_{l-1}$

This yields the recursion:

$$D_l \leq L_l^{(\theta)} B \Delta_l \cdot |\lambda - \lambda'| + L_l^{(h)} \cdot D_{l-1} \quad (33)$$

Step 3: Solving the Recursion. Let $\alpha_l = L_l^{(\theta)} B \Delta_l$ and $\beta_l = L_l^{(h)}$ for notational simplicity. The recursion becomes:

$$D_l \leq \alpha_l \cdot |\lambda - \lambda'| + \beta_l \cdot D_{l-1} \quad (34)$$

For the base case, we consider the embedding layer. If the embedding parameters are also interpolated, then $D_0 = \alpha_0 \cdot |\lambda - \lambda'|$ for some α_0 . Otherwise, $D_0 = 0$.

Unrolling the recursion:

$$D_L \leq \alpha_L |\lambda - \lambda'| + \beta_L D_{L-1} \quad (35)$$

$$\leq \alpha_L |\lambda - \lambda'| + \beta_L (\alpha_{L-1} |\lambda - \lambda'| + \beta_{L-1} D_{L-2}) \quad (36)$$

$$= (\alpha_L + \beta_L \alpha_{L-1}) |\lambda - \lambda'| + \beta_L \beta_{L-1} D_{L-2} \quad (37)$$

$$\leq \dots \quad (38)$$

$$\leq \left(\sum_{l=1}^L \alpha_l \prod_{j=l+1}^L \beta_j \right) |\lambda - \lambda'| + \left(\prod_{j=1}^L \beta_j \right) D_0 \quad (39)$$

Step 4: Final Bound. Defining:

$$C = \sum_{l=0}^L \alpha_l \prod_{j=l+1}^L \beta_j = \sum_{l=0}^L L_l^{(\theta)} B \Delta_l \prod_{j=l+1}^L L_j^{(h)} \quad (40)$$

we obtain:

$$D_L = \|h_\lambda^{(L)}(x) - h_{\lambda'}^{(L)}(x)\| \leq C \cdot |\lambda - \lambda'| \quad (41)$$

Since all terms $(L_l^{(\theta)}, L_l^{(h)}, B, \Delta_l)$ are finite constants, C is a finite constant, establishing Lipschitz continuity. \square

Remark 3 (Interpretation of the Constant C). *The constant C has a clear structure:*

$$C = \sum_{l=0}^L \underbrace{L_l^{(\theta)} B \Delta_l}_{\text{direct effect at layer } l} \times \underbrace{\prod_{j=l+1}^L L_j^{(h)}}_{\text{amplification through subsequent layers}} \quad (42)$$

Each layer contributes a term proportional to its parameter distance Δ_l , amplified by the Lipschitz constants of all subsequent layers. This explains why changes in middle-to-deep layers (where Δ_l is larger; as shown in Figure 2(c)) have stronger effects on the final representation.

Corollary 3 (Continuous Trajectory in Activation Space). *The mapping $\lambda \mapsto h_\lambda^{(L)}(x)$ is continuous. Moreover, the set $\{h_\lambda^{(L)}(x) : \lambda \in [0, 1]\}$ forms a connected path in activation space.*

Proof. Lipschitz continuity implies uniform continuity, which implies continuity. The image of a connected set $[0, 1]$ under a continuous function is connected. \square

Connection to Empirical Observations

Theorem 3 explains the PCA visualization in Figure 2(b):

1. **Continuous Trajectory:** The Lipschitz bound ensures that adjacent λ values produce nearby representations, resulting in the smooth curve observed in PCA space.
2. **Correlation with λ :** Since representation change is bounded by $C \cdot |\lambda - \lambda'|$, the dominant direction of variation aligns with the interpolation axis. This explains the high correlation ($r = 0.974$) between PC1 and λ .
3. **Proportional Spacing:** The roughly equal spacing between consecutive λ values in PCA space reflects the linear relationship between $|\lambda - \lambda'|$ and representation distance.

A.4 Benchmark Details.

MATHEMATICAL BENCHMARKS. We utilize a range of benchmark datasets to thoroughly evaluate model capabilities on mathematical reasoning tasks. These benchmarks cover a broad spectrum of difficulty levels, ranging from basic arithmetic operations to challenging competition-grade mathematics.

- **GSM8K** comprises 1,319 meticulously selected grade-school mathematics problems, intended to assess models' multi-step reasoning abilities in elementary mathematical contexts. Each problem generally involves two to eight successive operations, primarily grounded in fundamental arithmetic, and necessitates precise computation of intermediate values.

- **MATH-500** presents a demanding set of high-school-level problems spanning various mathematical domains, such as Prealgebra, Algebra, and Number Theory. These problems, largely derived from mathematics competitions, require both abstract reasoning and sophisticated logical inference. For consistency with previous studies, we use the 500-problem subset originally established by OpenAI as the evaluation standard.

- **AMC 2023** consists of 40 problems drawn from the 2023 American Mathematics Competitions (AMC), an annual event hosted by the Mathematical Association of America (MAA) that seeks to cultivate problem-solving abilities and discover mathematically talented students. The problems encompass fundamental areas including algebra, geometry, number theory, and combinatorics, providing a rigorous benchmark for assessing sophisticated mathematical reasoning.

- **AIME 2024 & 2025** include 60 challenging problems from the 2024 and 2025 editions of the American Invitational Mathematics Examination (AIME). This highly regarded competition tests participants' mathematical reasoning across a wide array of topics, encompassing arithmetic, algebra, counting, geometry, number theory, probability, and various other secondary school mathematics subjects.

VIDEO REASONING BENCHMARKS. To assess the model's ability to perform high-level logic, deduction, and expert-level analysis within video contexts, we employ the following benchmarks:

- **Holmes** (Video-Holmes) evaluates complex reasoning and active clue-seeking abilities within the mystery and detective genre. It features suspenseful clips where models must perform multi-hop deduction, detect anomalies, and integrate temporal clues to identify perpetrators and motives, simulating high-level cognitive deduction.
- **MMVU** is designed to assess expert-level disciplinary knowledge and reasoning in video understanding. It comprises 3,000 expert-annotated questions spanning four core disciplines—Science, Medicine, Humanities, and Engineering—requiring models to apply textbook-level academic knowledge to solve complex problems.
- **Video-MMMU** focuses on the capability of knowledge acquisition and transfer. Utilizing educational videos and lectures, it evaluates the "learning-to-answer" paradigm, measuring how well a model can perceive, understand, and apply new information learned from video content to solve novel questions.

GENERAL VIDEO UNDERSTANDING BENCHMARKS. We further evaluate the model's robustness in processing

diverse video durations and managing long-term contexts through these comprehensive benchmarks:

- **Video-MME** is a full-spectrum benchmark designed to assess multimodal analysis across varying durations, ranging from short clips to hour-long videos. It covers diverse domains such as movies and sports, integrating visual, audio, and subtitle modalities to test temporal reasoning and cross-modal alignment.
- **LVBench** targets extreme long-video understanding with high-quality content averaging over an hour in duration. It specifically challenges models’ long-term memory and information retrieval capabilities, requiring the extraction of specific entities and events from extensive and redundant temporal contexts.

MULTIMODAL MATHEMATICAL REASONING BENCHMARKS. To rigorously evaluate the intersection of visual perception and mathematical logic, we utilize datasets that range from diagnostic tests to expert-level challenges:

- **MMMU** evaluates expert-level multimodal reasoning across 30 heterogeneous disciplines, including engineering and clinical medicine. It demands deep domain knowledge to interpret complex visual data—such as chemical structures and medical imaging—combined with sophisticated logical inference.
- **MathVista** serves as an omnibus benchmark aggregating diverse mathematical tasks from 28 existing sources. It provides a holistic assessment of visual mathematical reasoning across a wide range of visual contexts, including geometry, function plots, and statistical charts.
- **We-Math** is a visual-centric benchmark constructed to address visual redundancy in existing datasets. It emphasizes fine-grained evaluation of multi-step reasoning where visual information is indispensable, serving as a diagnostic tool for true visual grounding in mathematical logic.
- **MathVision** is a large-scale, high-quality benchmark sourced from real-world mathematics competitions. Distinguished by rigorous data decontamination and high difficulty, it pushes the upper limits of current models by testing robust visual reasoning in complex, competition-grade scenarios.

B Hyperparameter Sensitivity Experiments

Hyperparameter Sensitivity of DAMI-Conf. Figure 10 investigates the effect of decision boundary μ and temperature τ on DAMI-Conf performance. The heatmap reveals that DAMI-Conf is robust across a wide range of hyperparameter configurations. The optimal performance is achieved at $\mu=0.3$ and $\tau=0.3$, which we adopt as default settings. Notably, the central region ($\mu \in [0.2, 0.4]$, $\tau \in [0.2, 0.4]$) consistently achieves above 89.5% accuracy, while extreme values at the boundaries lead to moderate degradation. This pattern is intuitive: overly small μ biases toward the Thinking model regardless of query difficulty, while overly large μ favors the Instruct model even for challenging queries. Similarly, extreme τ values either over-smooth or over-sharpen

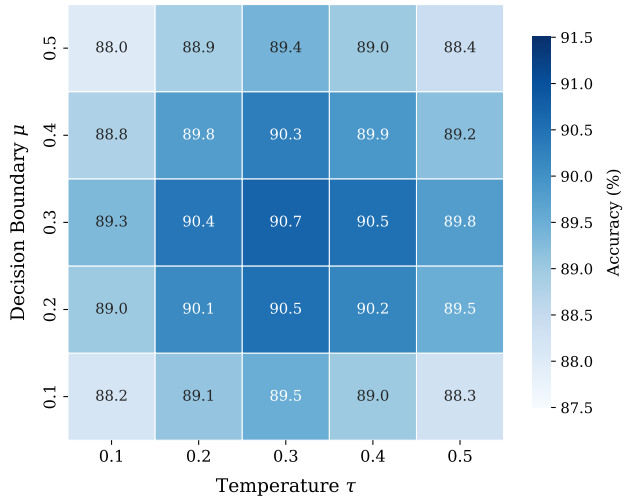


Figure 10: Investigation on the effect of hyperparameter μ and τ .

the λ distribution. The overall stability across configurations confirms that DAMI-Conf does not require careful hyperparameter tuning, making it practical for deployment without extensive validation.

C Rating Instruction of DAMI-Prompt Ethical Statement

There are no ethical issues.

Method	GSM8K			MATH-500			AMC			AIME24			AIME25			Overall		
	Acc↑	Tok↓	Think	Acc↑	Tok↓	Think	Acc↑	Tok↓	Think	Acc↑	Tok↓	Think	Acc↑	Tok↓	Think	Acc↑	Tok↓	Think
	2x	#N	#R	2x	#N	#R	4x	#N	#R	4x	#N	#R	4x	#N	#R	-	#N	#R
DAMI-Pref	94.5	843	25	96.4	4315	64	98.8	7872	86	85.0	15412	95	83.3	17488	92	91.6	9186	72
w/o Cost	94.0	1123	45	96.6	5102	78	98.8	8943	92	85.0	17821	98	83.3	19234	96	91.5	10843	82
DAMI-Conf	94.5	856	41	96.2	2954	34	98.8	5891	55	85.0	13485	79	79.2	16412	94	90.7	7919	61
w/o S_{ambi}	94.1	782	38	95.8	3127	39	97.5	5432	48	81.7	12876	72	75.0	15643	88	88.8	7572	57
w/o S_{dis}	94.0	889	44	95.4	2765	30	95.0	6102	58	80.0	14123	82	70.0	16892	95	86.9	8154	62
$\mathcal{C}^T(q)$ -only	93.6	945	48	94.6	3541	42	95.0	6834	64	76.7	14987	85	62.5	18231	97	84.5	8907	67

Table 2: Ablation study results on the (Qwen3-4B-2507-Thinking, Qwen3-4B-2507-Instruct) model pair.

Rate the difficulty of this math problem from 1 to 10 using these criteria:

Level 1-2 (Very Easy):

- Simple arithmetic (addition, subtraction, multiplication, division)
- Direct application of basic formulas
- Single-step problems

Level 3-4 (Easy):

- Multi-step arithmetic with 2-3 operations
- Basic word problems with clear solution path
- Simple algebra (solving for one variable)

Level 5-6 (Medium):

- Multi-step problems requiring 4+ operations
- Problems involving ratios, proportions, or percentages
- Systems of equations (2 variables)
- Geometry problems with standard formulas

Level 7-8 (Hard):

- Complex multi-step reasoning
- Abstract mathematical concepts
- Problems requiring creative problem-solving approaches
- Advanced algebra, combinatorics, or number theory

Level 9-10 (Very Hard):

- Competition-level mathematics
- Requires deep mathematical insight or multiple advanced techniques
- Abstract reasoning with non-obvious solution paths

Respond with ONLY a single digit (1-10) based on the problem's difficulty.

Problem: {question}

Difficulty rating:

Figure 11: Prompt template for difficulty rating in DAMI-Prompt.